

Surrogate impact modelling for crop yield assessment

O. Vlachopoulos¹, N. Luther¹, A. Ceglar³, A. Toreti², E. Xoplaki⁴

¹ Justus Liebig University Giessen, Giessen, Germany

² European Commission, Joint Research Centre, Ispra, Italy

³ Climate Change Centre, European Central Bank, Frankfurt am Main, Germany

⁴ CMCC Foundation - Euro-Mediterranean Center on Climate Change, Italy

Abstract

This study presents the Surrogate Engine for Crop Simulations (SECS), a group of deep-learning models that emulate the process-based ECroPS model using only daily maximum and minimum temperature and precipitation. In this study we emulate grain maize and spring barley. Trained on ERA5-forced ECroPS simulations, SECS reproduces crop growth dynamics and harvest timing with high fidelity. Critically, SECS extremely reduces computational costs enabling ensemble-scale inference suitable for operational pipelines.

When driven by seasonal data, SECS captures the interannual and spatial patterns of crop stress across Europe and aligns with independent monitoring, supporting its use as a probabilistic Areas of Concern indicator for early warning. Under CMIP6 scenarios (SSP3-7.0 and SSP5-8.5), SECS consistently identifies the Mediterranean basin as a persistent hotspot of yield risk through mid-century, with central–northern Europe showing mixed signals. These results demonstrate that a streamlined, data-efficient emulator can provide robust seasonal-to-climate risk assessments at continental scale.

Main

Crop growth modeling serves as a foundational tool for developing comprehensive spatiotemporal insights, supporting crop yield prediction and risk assessment under climate change conditions and scenarios as well as for optimizing agricultural practices¹. Sophisticated crop growth models, such as ECroPS (Engine for Crop Parallelizable Simulations), WOFOST (World Food Studies)^{2,3} and APSIM (Agricultural Production Systems sIMulator)⁴ are instrumental in simulating and assessing crop performance under diverse and changing environmental conditions^{5,6}. These models incorporate intricate biological, physiological, and environmental dynamics, and agricultural management decisions to realistically simulate crop growth and development over varying temporal scales^{7,8}.

In the context of ongoing climate change, crop growth models are vital for assessing the vulnerability, resilience, and adaptive capacities of agricultural systems. By simulating various future climate scenarios and evaluating their potential impacts on crop growth and agricultural

productivity, these models deliver essential data for designing robust climate adaptation and mitigation strategies. Specifically, they enable detailed evaluations of how different crop varieties, cropping systems, and agricultural management practices respond to anticipated shifts in temperature, rainfall patterns, and the frequency and intensity of extreme weather events^{9–12}.

Today artificial intelligence (AI) is emerging as a powerful complement to traditional mechanistic crop models introducing transformative approaches capable of efficiently simulating complex agricultural systems^{13–15}. Unlike mechanistic models that depend on predetermined equations and theoretical assumptions, AI-based models can derive insights directly from extensive datasets¹⁶ while accommodating representations of mechanistic or empirically-driven dynamics¹⁷. This ability to identify nonlinear, intricate relationships among various environmental factors and crop responses can significantly enhance predictive accuracy and modeling flexibility¹⁸.

A major advantage of AI-driven models lies in their computational efficiency and scalability, making them particularly suitable for large-scale applications, scenario testing and real-time decision-making. Leveraging parallel computing and distributed processing capabilities, AI approaches facilitate rapid analysis of extensive datasets, enabling faster scenario evaluations and sensitivity assessments than traditional methods¹⁹. AI applications like surrogate modeling and emulation have emerged as robust methods for enhancing the calibration, validation, and uncertainty quantification of complex processes from economy²⁰ to agroecosystems²¹. By training AI models to replicate the behavior of computationally intensive simulations, researchers can develop lightweight, interpretable emulators²².

Given the complexity and resource-intensive nature of our current focus, ECroPS, we are operationalizing crop growth modeling by developing an AI-based surrogate model which can reduce inherent uncertainties tied to the process-based modelling abstractions of complex systems²³ and enable ensemble runs, resulting in statistically robust, probabilistic analyses.

In recent works related to surrogate modelling of crop growth, the main focus is the emulation of yield output; using a series of independent variables in order to replicate the target variable. These works are either hybrids or pure AI-driven models. In terms of hybrid process-based and ML-driven modelling, Shahhosseini et al.²⁴ showed that coupling a process-based model with ML improves maize yield prediction. They ran the APSIM crop model to generate features (e.g. soil moisture, crop stress indices) and fed these into various machine learning (ML) algorithms (linear regression, LASSO, random forests, XGBoost, etc.). This hybrid approach outperformed standalone models and showcased that integrating mechanistic crop model insights with ML boosted accuracy and generalizability of yield forecasts. Zhang et al.²⁵ used ensemble modelling of XGBoost and Random Forests to emulate yield using 20 predictors such as agro-climatic indices, soil attributes, geographical features among others, delivering maize yield predictions while exploring the impact of future climate conditions. Liu et al.²⁶ developed ML-based statistical surrogates to replicate year-to-year yield variability under various scenarios using an XGBoost-based approach. While informative, these studies overlook the full time series of crop development, insufficiently capture weather impacts between critical phenological phases due to their loss of memory-driven dynamics, and rely on coarse temporal resolution, while being highly input-intensive. Additionally, most of the approaches towards a crop model surrogate lack the potential of being able to extend towards an actual climate service. Such a characteristic is central to this study.

Results

In this study we emulate with distinct AI models the crop growth for two European core crops, grain maize and spring barley. SECS is built for Maize (SECS4M) and for Spring Barley (SECS4SB).

Grain maize is a vital crop within the EU primarily utilized for animal feed, human consumption and biofuel production²⁷. In 2023, EU grain maize and corn-cob-mix production reached approximately 61.0 million tons ($\approx 22.5\%$ of total EU cereals output), representing a 15.2% increase compared to the drought-affected 2022 season, despite a 6.1% reduction in harvested area to 8.3 million hectares²⁸. Barley, including spring barley sown in spring, is another core EU cereal, widely used as animal fodder and as a key input for malting (beer/whisky). In 2023 the EU harvested around 47 million tons of barley ($\approx 17.4\%$ of total cereals output), and the overall barley area was broadly stable at around 10 million hectares.

We emulate crop growth utilizing various climate data from Earth System Models (ESMs) from the Coupled Model Intercomparison Project Phase 6 (CMIP6, Table A1), the European Centre for Medium-Range Weather Forecasts (ECMWF) Seasonal Forecast System 5.1 (SEAS5.1)²⁹ and ECMWF ReAnalysis, version 5 (ERA5)³⁰, which also serves as the benchmarking force.

The CMIP6 data were bias adjusted using ERA5 reference data (1940-2014) and the quantile delta mapping (QDM) methodology³¹ using the MBC R-package. The SEAS5.1 data were also bias adjusted with ERA5 using the hindcast ensemble pool for the period (1993-2016) as reference for the QDM correction process.

Performance

The SECS group of models is trained on ERA5-forced yearly crop yields from ECroPS for the years 1993 to 2023. More specifically, the crop yield target variable is the Total Weight of Storage Organs (TWSO), under water-limited conditions. The temporal resolution is daily, while on the spatial domain the model is agnostic, and like ECroPS, it runs at the grid cell level. TWSO is measured in kilograms per hectare (kg ha^{-1}).

Computational performance

SECS demonstrates excellent computational efficiency, making it well-suited for large-scale, operational use. On Deutsches Klimarechenzentrum (DKRZ, German Climate Computing Centre) Levante high-performance computing (HPC) system, SECS requires approximately 0.008 seconds of CPU time to generate a yield prediction for a single grid cell over one year. In contrast, the ECroPS model, with its detailed mechanistic simulations, requires around 70 seconds of CPU time for the same task, making it roughly four orders of magnitude slower.

Goodness of fit of SECS

SECS evaluation lies in a two-stage process: Firstly, the actual training and testing process, using the ECroPS attainable TWSO output (using ERA5 and the static EC-JRC gridded datasets) to train and test the prediction pipeline. Secondly, once the AI surrogate is trained, and since ECroPS cannot be directly utilized with SEAS5.1 or CMIP6 weather data due to the lack of

common resolution inputs for soil characteristics, crop-specific grids and agro-management data, the evaluation is performed between the ERA5-forced benchmark AI model output and the target AI surrogate yield (using SEAS5.1 or CMIP6). To evaluate SECS performance on the testing dataset, the Fréchet and the Hausdorff distances as geometric similarity metrics were applied. The results of the comparison of the test dataset with the corresponding ground truth from ERA5-driven ECroPS simulations are shown in Figure A1. Figure 1 shows random crop growth evolution sample cells. It is apparent that the model performance is very good, with the emulator capturing accurately both the evolution of the crop and the maturity.

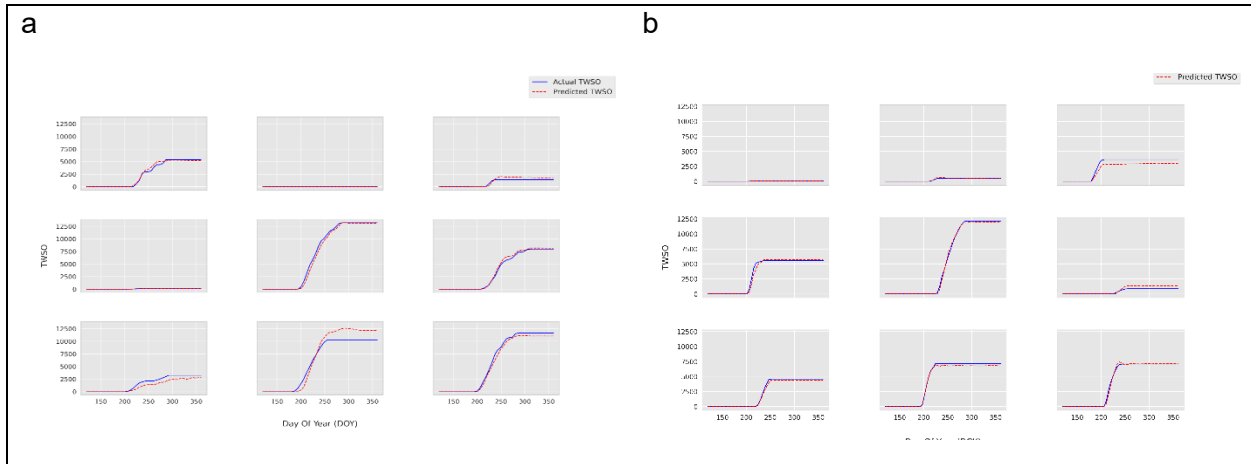


Figure 1: Random samples (grid points) of grain maize (a) and spring barley (b) crop growth timeline in terms of actual and predicted TWSO (kg ha^{-1})

Forcing SECS4M with SEAS5.1 and CMIP6

We demonstrate the outputs for grain maize as a major crop showcase. SECS4M is evaluated and analysed by comparing yield outputs forced with SEAS5.1 and CMIP6 climate inputs (historical baseline) against reference yields obtained by ERA5 forcing. Representative examples of the performance metrics employed in this assessment are presented below, with the same evaluation procedure applied uniformly across all datasets considered.

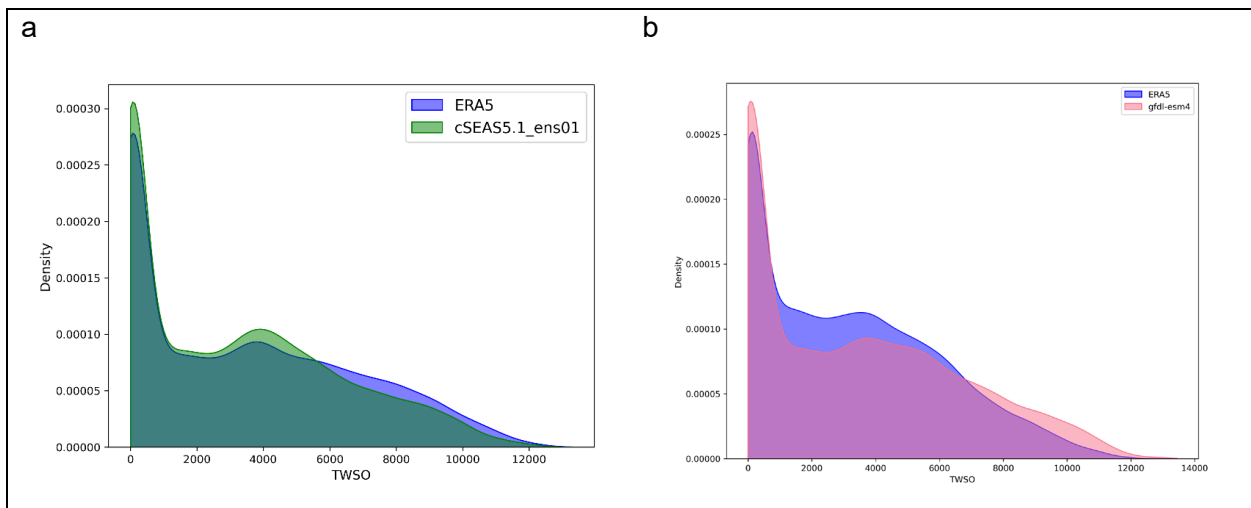


Figure 2: Overlaid probability density functions of TWSO (kg ha^{-1}) SECS4M simulations forced with ERA5 and (a) cSEAS5.1 ensemble member 01 (cSEAS5.1_ens01), (b) GFDL-ESM4 (r1i1p1f1) for 1993-2014

SEAS5.1

Crop yield simulations using SEAS5.1 are produced with the surrogate model for both the reforecast period (1993–2016), comprising 25 ensemble members, and the forecast period (2017–2023), comprising 51 ensemble members. The case study here analysed focuses on the seasonal forecast that bursts in June 2022 as it was a year with heavy damages in the production of grain maize ³². SECS4M was forced with a concatenated dataset of ERA5 (January to May) and the bias adjusted SEAS5.1 (June to December), henceforth named cSEAS5.1, in order to simulate a full year of grain maize in an operational manner when the required forecast data to run the full crop growth simulation would be released. The summer months in the seasonal forecast comprise lead times 0, 1 and 2, which is an important aspect of the use-case methodology since those months are most impactful for crop growth due to intense droughts and heatwaves and the skill of the forecast is highest at lead time 0, progressively getting lower per lead time.

Figure 2a shows the probability density comparison between the ERA5 and the cSEAS5.1 ensemble member 01 -forced TWSO suggesting minor differences in how the reanalysis and bias adjusted seasonal forecast models capture extreme and intermediate TWSO conditions, while exhibiting a common structure and density outline.

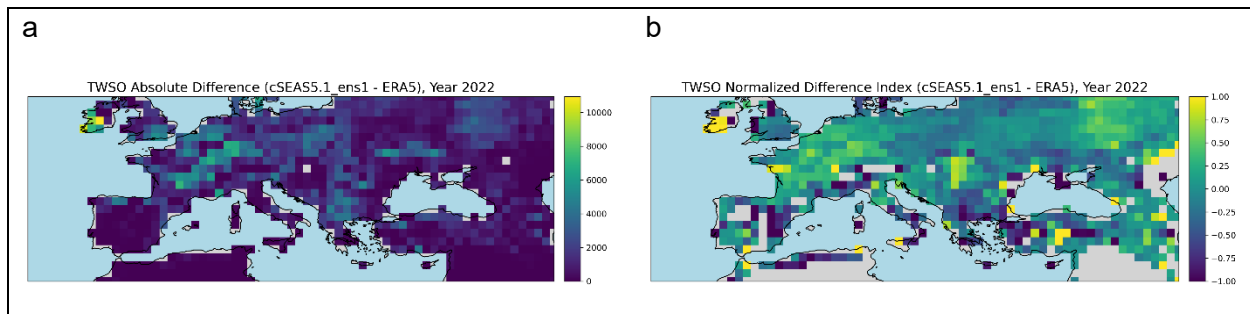


Figure 3: Comparison of the ERA5 and cSEAS5.1_ens01 TWSO SECS4M simulations for year 2022: (a) Absolute difference in kg ha^{-1} and (b) Normalized Difference Index.

In Figure 3 we see the maps of two metrics used to assess the spatial skill of the cSEAS5.1_ens01-forced TWSO relative to the ERA5-forced TWSO, the absolute difference and the Normalized Difference Index (NDI), which bounds the error in $[-1, 1]$. The two maps summarize how the 2022 TWSO differs when ECroPS is driven by ERA5 versus cSEAS5.1 (ens1). The absolute-difference panel shows that most grid cells over Europe have relatively small deviations indicating broad consistency between the two forcings, but with distinct, spatially coherent patches with high discrepancies. These hotspots occur in scattered belts across western–central Europe and parts of eastern and southeastern Europe, as well as at a few coastal grid cells, suggesting localized sensitivity to differences in e.g., precipitation or heat stress, rather than a domain-wide offset. The NDI reveals that cSEAS5.1 tends to produce higher TWSO than ERA5 across much of northern and north-eastern Europe, while lower values relative to ERA5 dominate large parts of the Iberian Peninsula, the central and southern Mediterranean rim (including Italy and the Balkans), and portions of the eastern Mediterranean. Together, the two plots indicate that (i) magnitude disagreements are generally modest but feature isolated peaks, and (ii) the sign of the difference is not random as there is a north–south dipole with cSEAS5.1 favoring higher yields in cooler/wetter regions and ERA5 favoring higher yields in warmer/drier zones for this year.

Notably for Figure 3 and henceforward, the area of Northern Africa and the eastern parts of the map that have no values or concentrated zeros are grid cells that do not have TWSO calculated and are outside the scope.

CMIP6

For the CMIP6 models, we fed SECS with the historical simulations summarized in Table A1, generating yield outputs for 1993–2014, using the same evaluation window as with SEAS5.1. This period provides a stable basis for agricultural activity, minimizing impacts from major shifts in management practices and production systems.

Representative evaluation metrics are shown in the following figures derived from forcing the SECS4M model with GFDL-ESM4 as a showcase.

In Figure 2b both datasets exhibit a strongly right-skewed distribution with a sharp mode at low TWSO and a long upper tail. Relative to ERA5-forced TWSO, GFDL-ESM4-forced TWSO places slightly more probability mass at very low values ($< \sim 1,000 \text{ kg ha}^{-1}$) and shows a heavier upper tail that extends beyond $\sim 10,000\text{--}13,000 \text{ kg ha}^{-1}$, indicating a greater incidence of high TWSO outcomes. ERA5 has comparatively higher density in the mid-range ($\sim 2,500\text{--}5,000 \text{ kg ha}^{-1}$).

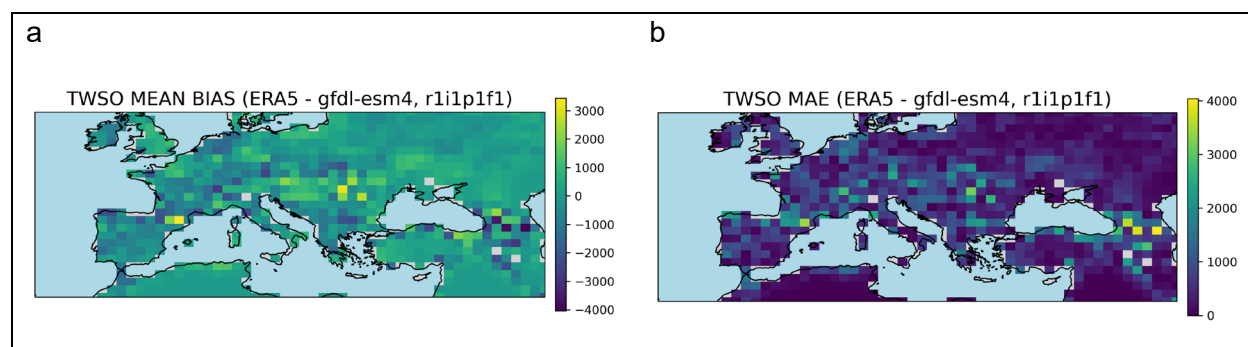


Figure 4: Comparison of the ERA5 and GFDL-ESM4 (r1i1p1f1) SECS4M simulations over the period 1993-2014: (a) Mean bias; (b) Mean Absolute Error

In Figure 4, climatological error maps show generally small values across much of western and central Europe, with localized hotspots where both metrics rise approaching $\sim 3,000\text{--}4,000 \text{ kg ha}^{-1}$. The mean-bias map (ERA5 – GFDL-ESM4) indicates a weakly positive bias over large areas, but with mixed-sign, high-magnitude biases clustered in the eastern parts of Europe, pointing to spatially heterogeneous, regionally coherent offsets. The co-occurrence of large bias with elevated Mean Absolute Error (MAE) suggests that systematic offsets are a major contributor to the error in those hotspots. These spatial patterns are consistent with the PDF comparison, where GFDL-ESM4 places slightly more probability at very low TWSO and exhibits a heavier upper tail than ERA5, i.e., a broader spread that manifests geographically as mixed-sign biases and larger magnitude errors in specific regions (all statistics are computed per grid cell across the full 1993–2014 period).

Areas of Concern

cSEAS5.1

AoC detection for cSEAS5.1-forced surrogate yields follows a tercile-based probabilistic protocol. In Figure 5 we show for year 2022 the most-probable category of TWSO anomaly from the cSEAS5.1 ensemble at each grid cell, based on terciles derived from the 1993–2016 reference.

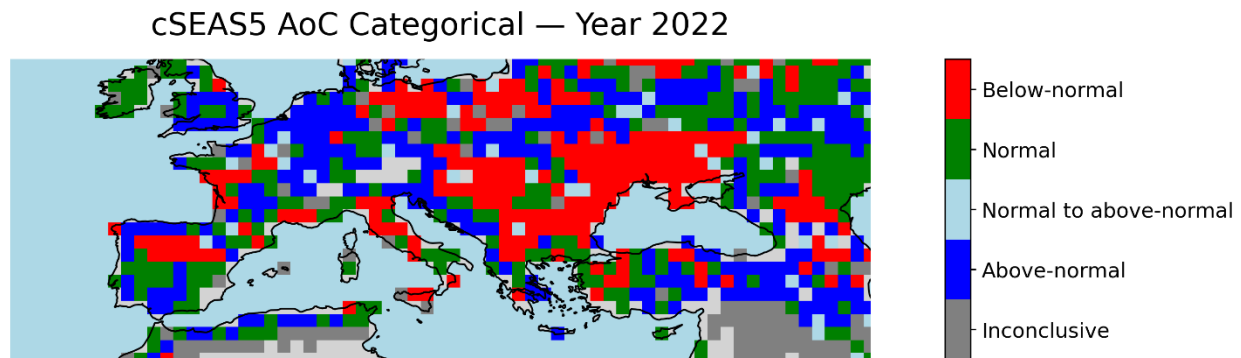


Figure 5: Probabilistic Areas of Concern for grain maize, year 2022 based on 51 ensemble members of cSEAS5.1

The 2022 AoC map for grain maize forms a broad west–central to south-eastern belt—spanning much of France, Italy, the Carpathian Basin (Hungary, Romania, Serbia), and parts of central–eastern Europe—while the Atlantic northwest (UK/Ireland), parts of Scandinavia/Baltics, and irrigated basins in Spain/Portugal are mostly normal to above-normal. This pattern aligns with contemporaneous monitoring: JRC MARS bulletin in summer 2022 flagged sharply reduced yield outlooks for grain maize across France, Italy, and central–eastern Europe; Copernicus ESOTC³³ documented widespread agricultural impacts from the spring–summer drought and heat; and the European Commission’s autumn outlook recorded the steepest EU-wide production decline among major cereals for grain maize (mainly Italy, France, and the Balkans/Central Europe). Overall, the AoC map agrees well with independent reports on where maize stress and damage were concentrated in 2022^{32,34–37}.

CMIP6

We carried out the AoC analysis for CMIP6 models using multiple realizations under SSP3-7.0 and SSP5-8.5 (Table A2). Each model provides a simulation to 2050 and a matching historical run, which also acts as the reference yield baseline used to compute relative anomalies. In order to conduct a meaningful study we assume that agricultural production remains as-is, without the impact of mitigation and resiliency strategies. This is a key factor which limits the time horizon to 2050, as further on, any analysis with such an assumption for agricultural production would be very far from any possible reality.

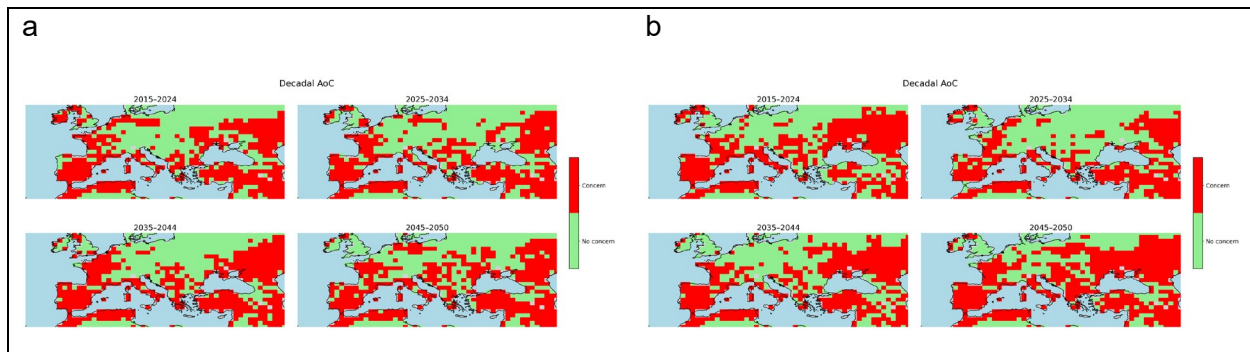


Figure 6: Grain maize 10-yearly average AoC maps for GFDL-ESM4 derived TWSO under (a) SSP3-7.0 and (b) SSP5-8.5

SSP3-7.0

In Figure 6a and under SSP3-7.0 for GFDL-ESM4, the decadal AoC signal is persistently Mediterranean-centric. In 2015–2024, widespread AoC span within Iberia, southern France, Benelux, Italy, the Balkans, Turkey, surrounding the Black Sea, with incursions along the Atlantic front, while a broad central–eastern European area remains largely of no concern. The pattern holds in 2025–2034: the Mediterranean areas stay red, but the green “no-concern” spine from France/Germany to Poland and western Ukraine persists, despite scattered red tiles along coastal/land–sea contrast zones.

A step change occurs in 2035–2044, when AoC expand inland to form a near-continuous corridor from Iberia through the northern Mediterranean and Balkans to the southern coast of the Black Sea; only northern Europe and a small central Black Sea pocket remain predominantly of no concern. By 2045–2050, a north-central corridor of the UK, northern France/Germany/Poland and western Ukraine, returns to “No concern”, yet the Mediterranean arc remains consistently in concern. Overall, the AoC footprint peaks in 2035–2044 and shows partial relief by mid-century, but the Mediterranean cropping systems remain the most exposed throughout.

SSP5-8.5

Under SSP5-8.5 for GFDL-ESM4 from 2015–2024 (Figure 6b), a strong Mediterranean-centric signal is in place: AoC dominate Iberia, southern France, Italy, Balkans, parts of Turkey and extends along the Black Sea with an epicenter in SW Russia and Ukraine. A broad central–eastern European corridor remains mostly of no concern. In 2025–2034, the Mediterranean arc shows persistent stress while the France/Germany to Poland/Ukraine spine largely retains “No concern”. Red tiles spread sporadically into western and central Europe, beyond the Mediterranean corridor. A marked inland expansion appears in 2035–2044, yielding a near-continuous AoC corridor from Iberia through the Mediterranean and Balkans to the southernmost Black Sea region, with “No concern” persisting mainly over northern Europe and isolated pockets around the central Black Sea. By 2045–2050, a north-central corridor (determined by UK, N. France/Germany/Poland and Ukraine) returns to “No concern”, but the Mediterranean arc remains consistently red. Compared with SSP3-7.0, SSP5-8.5 tends to show a more persistent and contiguous AoC footprint, especially across the eastern Mediterranean and Black Sea rim, underscoring heightened mid-century risk for Mediterranean cropping systems and those surrounding the Black Sea.

Discussion

This study presents SECS, an AI-based emulator that reproduces the outputs of the mechanistic ECroPS model while cutting computational cost by ~four orders of magnitude. Using only daily minimum/maximum temperature and precipitation, SECS is scalable and operationally feasible for crop forecasting and climate-service pipelines. The large speed-up enables rapid, repeated yield prediction, supporting ensemble forecasts and real-time or near-real-time agricultural decision-making when required. SECS is therefore suitable for digital twins, operational climate services and early-warning systems.

Key contributions are: (1) accurate yield prediction under water-limited conditions, capturing crop-growth dynamics and maturity timing in strong agreement with ECroPS; (2) efficiency that makes ensemble-based probabilistic forecasting practical for uncertainty assessment and identifying AoC; (3) validation with cSEAS5.1 seasonal forecasts, which SECS uses to reproduce reported spatiotemporal patterns of crop stress; and (4) robustness for long-term risk assessment using CMIP6 projections under SSP3-7.0 and SSP5-8.5, e.g. consistently flagging the Mediterranean as a persistent vulnerability hotspot.

For decision-making, SECS operationalizes continental-scale yield forecasting to inform adaptation (e.g., sowing-date shifts, stress-tolerant cultivars, improved resource management). It also advances surrogate modelling by showing nested LSTMs can emulate complex mechanistic models with operational utility.

Caveats include dependence on training simulations (potential weakness under underrepresented extremes), reduced mechanistic transparency relative to ECroPS, and regional specificity (EC-JRC valid cells), limiting transferability. Future work may extend to other crucial crops such as winter wheat, incorporate nutrient limits and management, and couple SECS with real-time Earth observation and high-resolution forecasts to strengthen risk-assessment and early-warning performance in an increasingly uncertain climate.

Methods

Input streams

We effectively simulate daily maize and spring barley growth dynamics with ECroPS spanning the period from 1993 to 2023 in the region (used by the European Commission Joint Research Centre, EC JRC, for its MARS Crop Yield Forecasting System³⁸) extending from 17.19° W to 48.99° E and from 32.76° N to 56.01° N. The model is calibrated to account for the spatial variability in crop model parameters across Europe, thus considering different spatial variety distribution for the main crops¹⁰. The latter is based on pan-European spatial calibration of several crop parameters relating to variety prevalence in different European growing regions. ECroPS distinguishes three levels/choices of crop growth simulations: potential production, water-limited production (water availability limits potential production) and nutrient limited production (in which nutrient availability limits water-limited production). This study focuses on the water-limited

production setup to demonstrate the benefits and the performance of the AI emulator. Of course, it can be extended to other simulation settings.

In terms of weather, six daily variables are used for the simulations: maximum temperature, minimum temperature, shortwave downwelling radiation at the surface, total precipitation, relative humidity, and wind speed derived from vector components.

The input data considering soil characteristics are gridded static data derived from the databases of the EC-JRC. Accordingly, the European soil is divided into soil mapping units (SMU) representing differentiated zones that reflect the soil types' homogeneity. The original soil database SMUs consist of one or more soil types, represented with soil typological units (STUs), with STUs occupying measured percentages per SMU. Overall, the provided soil map used for crop growth determine aspects such as the rooting depth, the available water capacity and the infiltration capacity, variables that are associated with the STU and are therein introduced as soil moisture characteristics. Without losing the generalizability of our methodology, we avoid introducing the complexity of accounting for the possibly multiple STUs associated with every grid cell of the European domain, and thus requiring as many simulations as the STUs per grid cell. Instead, we perform the simulations per grid cell by using the most dominant soil type.

Finally, crop-specific data and agro-management information per cell are utilized. Sowing date and number of degree-days for the emergence-anthesis period and the number of degree-days for the anthesis-maturity period, vernalization parameters, dry matter partitioning parameters and many others, required for the simulation runs for grain maize are provided by EC-JRC.

We consider crop and soil parameters stationary while ERA5 variables are the time-varying components that force the ECroPS model between 1993 and 2023. Each cell output is an independent simulation, forced from sowing date to the end of each year, producing output variables such as the Attainable TWSO on a daily basis as the crop grows.

In terms of model runs, the surrogate streamlines input requirements, relying solely on three critical meteorological variables: daily minimum temperature, daily maximum temperature, and daily total precipitation. These variables are selected due to their direct impact on crop stress factors, simplifying the modeling process and reducing forecast uncertainties inherent in the six-variable input requirements of ECroPS. Consequently, our AI-based emulator facilitates computationally efficient and highly scalable crop yield simulations, enhancing their integration into practical decision-support tools.

AI pipeline, architecture and feature engineering

SECS employs advanced deep learning methodologies to effectively model the complex, nonlinear, and dynamic relationships between environmental variables and crop growth responses. This approach addresses the significant computational complexity and resource-intensive nature that often restricts broader adoption of traditional mechanistic crop models.

Utilizing state-of-the-art computational capabilities such as parallel GPU processing and distributed computing, SECS swiftly processes large datasets, trains the surrogate model efficiently, and generates rapid predictions. These features facilitate real-time agricultural decision-making and robust risk assessment strategies. By accurately emulating the behavior of

conventional, computationally demanding simulations at a fraction of the cost, SECS enhances the integration of crop growth modeling into practical decision support frameworks, empowering stakeholders to manage agricultural systems proactively under uncertain environmental conditions.

SECS's modeling foundation is Recurrent Neural Networks (RNNs), a specialized neural network architecture tailored for sequential data analysis. Unlike conventional feedforward neural networks, RNNs incorporate feedback loops enabling the retention and utilization of historical data, making them exceptionally effective for tasks involving temporal dependencies, including time series forecasting and the simulation of dynamic agricultural systems. This inherent ability to capture temporal patterns solidifies RNNs as critical components in applications where understanding and forecasting dynamic processes are essential.

Building upon the foundational Recurrent Neural Network (RNN) architecture, Long Short-Term Memory (LSTM) networks were developed to overcome common challenges such as the vanishing gradient problem by employing gating mechanisms that control information flow³⁹. Advancing this concept further, nested LSTM networks incorporate hierarchical memory structures by embedding LSTM cells within other LSTM cells. This design enables the network to capture multiple temporal abstraction levels, effectively modeling detailed short-term fluctuations and broader long-term trends simultaneously. The hierarchical memory concept was notably advanced by Chung, Ahn and Bengio⁴⁰, who introduced hierarchical multiscale recurrent neural networks, laying the groundwork for sophisticated modeling approaches.

For training and evaluating SECS, the dataset is partitioned into training (90%) and testing (10%) subsets. Each dataset sample represents a specific location, incorporating daily weather observations as independent variables spanning multiple years, with ECroPS-simulated maize yield serving as the dependent variable. The primary features used by the surrogate model include daily maximum and minimum temperatures, total precipitation, and engineered variables such as temporally lagged weather conditions and the day of the year (DOY).

The incorporation of lagged features is crucial, offering historical weather context that enhances predictive accuracy. Lagged variables leverage three core rationales: (i) the persistence of weather regimes, (ii) delayed crop responses resulting from cumulative impacts of temperature and precipitation, and (iii) improved capacity to recognize reoccurring sequential weather phenomena, such as dry spells followed by rainfall. For each day analyzed, the dataset integrates weather conditions from the previous one to five days, thereby enabling the model to link past weather dynamics effectively to future yield trends.

Time-series AI models, such as RNNs, require structured input sequences to effectively capture meaningful temporal relationships. In SECS, fixed-length, 6-day batches are employed to capture both short-term variability and longer-term dependencies across multiple sequences. This batching method ensures each sample encompasses a meaningful temporal window, enabling the model to identify localized fluctuations in environmental variables while maintaining broader temporal trend awareness. Using non-overlapping sequences prevents redundancy and ensures independence among batches, enhancing the model's learning accuracy. The choice of a 6-day window delivers an optimal balance, providing sufficient context for modeling critical weather-driven dynamics relevant to crop development.

This batching technique is especially critical for the nested RNN architecture. It allows inner LSTM units to identify intricate, short-term patterns within each batch, while outer LSTM units capture broader trends across sequential batches. Such hierarchical partitioning enables the efficient processing of temporal dependencies at multiple scales, significantly enhancing pattern recognition and predictive capabilities.

SECS is structured hierarchically to effectively process sequential time-series data, as illustrated in Figure A2. The architecture comprises two LSTM levels: an inner TimeDistributed LSTM captures detailed short-term patterns within each 6-day batch, and an outer LSTM processes the aggregated outputs from these batches, effectively modeling long-term dependencies. The inner LSTMs distill short-term variability into concise representations, which the outer LSTMs utilize to track evolving temporal relationships between batches. This design ensures accurate identification of the dynamics of crop growth, resulting in sequential yield predictions.

The final predictive step utilizes a TimeDistributed dense layer wrapped with a Rectified Linear Unit (ReLU) activation function to preserve the sequential nature and ensure non-negative output values, aligning with the practical requirements of yield data. A dropout layer with a dropout rate of 0.3 is included to mitigate potential overfitting.

The surrogate model training employs the Adam optimizer⁴¹, with each LSTM layer containing 128 units. Additionally, the Huber loss function⁴² with a loss delta of 0.5 is utilized for stable training, providing robustness compared to traditional MAE.

All modeling components are implemented using Python (version ≥ 3.7) within the TensorFlow Keras framework^{43,44}.

To evaluate SECS performance on the testing dataset, two geometric similarity metrics were applied: the Fréchet distance⁴⁵, which captures both spatial and temporal correspondence between predicted and observed sequences, and the Hausdorff distance⁴⁶, which quantifies the maximum spatial deviation irrespective of temporal order. The Fréchet distance reflects discrepancies in shape, magnitude, and timing, providing a holistic assessment of dynamic similarity, whereas the Hausdorff distance emphasizes worst-case mismatches and structural outliers. Together, they offer complementary perspectives on model fidelity in reproducing the temporal and structural characteristics of the reference data.

Additionally, we assess the agreement between ERA5-forced and CMIP6- or SEAS5.1-forced TWSO using a probability-density comparison overlaying probability density functions using kernel density estimators for TWSO using all available grid cells and time steps. In the representation, the vertical axis is a probability density, allowing comparison of central tendency, spread, and tail behavior. Additionally, we compute error maps showing metrics such as the MAE and the mean bias.

Areas of Concern

The SECS output for TWSO is additionally utilized to determine Areas of Concern (AoC). AoC represent specific regions that are susceptible to significant agricultural impacts due to climate/weather extremes and/or unfavorable conditions, requiring targeted monitoring and management interventions. The EC-JRC employs a similar concept to highlight areas at risk of

substantial yield declines, crop failures, water deficits, and drought conditions^{47,48}. Identifying AoC serves as a strategic forecasting tool, guiding research priorities, preparedness and mitigation strategies.

Within this study, we adopt a simplified AoC concept than the one used by EC-JRC. The AoC methodology highlights the capabilities of operational crop forecasting systems, providing a useful climate service for future agricultural seasons. Specifically, AoC are identified based on impact classification derived from the SECS4M outputs, defining regions as AoC if they exhibit at least a 5% yield reduction compared to mean yields from a defined reference period. In terms of ensemble forecasting, such as for surrogate yields driven by SEAS5.1, the identification of AoC relies on a probabilistic approach. The reference yields are derived from the full ensemble of reforecasts spanning 1993 to 2016. Initially, the method computes the mean TWSO across all ensemble members and the entire reference period. Deviations from this baseline are calculated as relative anomalies, expressed as a percentage change relative to the reference values, with only negative anomalies retained. Dynamic thresholds for classifying these anomalies are established by calculating the lower (33rd percentile) and upper (66th percentile) terciles from the relative anomalies across the reference ensemble.

For the forecast period (2017–2023), relative anomalies are similarly computed using the same baseline, again retaining only negative values. Each forecasted ensemble member's anomaly is categorized as follows: anomalies exceeding the upper tercile threshold are classified as above-normal, anomalies between the upper and lower terciles as normal, and those below the lower tercile as below-normal. Subsequently, the probability of each category occurring is quantified based on the percentage of ensemble members classified accordingly.

Finally, decision rules are established to assign the most probable forecast category to each grid cell and forecast timestep. These decision rules are: (i) inconclusive if probabilities of below-normal and above-normal are equal; (ii) above-normal when above-normal probability exceeds the others; (iii) normal to above-normal when above-normal and normal probabilities are equal; (iv) normal if normal probability surpasses others; and (v) below-normal when below-normal probability is highest. This structured decision-making framework enhances the accuracy and reliability of identifying AoC and guides targeted interventions and preparedness strategies.

Author Contributions

Conceptualization, O.V., N.L., A.C., A.T. and E.X.; Data curation, O.V.; Investigation, O.V., N.L. and E.X.; Methodology, O.V.; Software, O.V.; Writing-original draft, O.V.; Writing-review and editing, O.V., A.C., A.T., E.X. . All authors have read and agreed to the published version of the manuscript.

Acknowledgments

The authors would like to thank Stefan Niemeyer (EC-JRC) and Davide Fumagalli (EC-JRC) for their support in providing crop-related data for ECroPS. O.V., N.L. and E.X. acknowledge support

from the Horizon 2020 project CLINT (number 101003876) and the German Federal Ministry of Research, Technology and Space (BMFTR) project ClimXtreme II.

References

1. Sweet, L. *et al.* Transdisciplinary coordination is essential for advancing agricultural modeling with machine learning. *One Earth* **8**, 101233 (2025).
2. de Wit, A. *et al.* 25 years of the WOFOST cropping systems model. *Agric. Syst.* **168**, 154–167 (2019).
3. van Diepen, C. a., Wolf, J., van Keulen, H. & Rappoldt, C. WOFOST: a simulation model of crop production. *Soil Use Manag.* **5**, 16–24 (1989).
4. Holzworth, D. P. *et al.* APSIM – Evolution towards a new generation of agricultural systems simulation. *Environ. Model. Softw.* **62**, 327–350 (2014).
5. Li, X. *et al.* Sensitivity Analysis of the WOFOST Crop Model Parameters Using the EFAST Method and Verification of Its Adaptability in the Yellow River Irrigation Area, Northwest China. *Agronomy* **13**, 2294 (2023).
6. Zhai, Z., Martínez, J. F., Beltran, V. & Martínez, N. L. Decision support systems for agriculture 4.0: Survey and challenges. *Comput. Electron. Agric.* **170**, 105256 (2020).
7. Toreti, A., Cronie, O. & Zampieri, M. Concurrent climate extremes in the key wheat producing regions of the world. *Sci. Rep.* **9**, 5493 (2019).
8. Toreti, A. *et al.* Climate service driven adaptation may alleviate the impacts of climate change in agriculture. *Commun. Biol.* **5**, 1235 (2022).
9. Abramoff, R. Z. *et al.* Adaptation Strategies Strongly Reduce the Future Impacts of Climate Change on Simulated Crop Yields. *Earths Future* **11**, e2022EF003190 (2023).
10. Ceglar, A. *et al.* Improving WOFOST model to simulate winter wheat phenology in Europe: Evaluation and effects on yield. *Agric. Syst.* **168**, 168–180 (2019).
11. Srivastava, A. K. *et al.* Modelling mixed crop-livestock systems and climate impact assessment in sub-Saharan Africa. *Sci. Rep.* **15**, 1399 (2025).

12. Timlin, D., Paff, K. & Han, E. The role of crop simulation modeling in assessing potential climate change impacts. *Agrosystems Geosci. Environ.* **7**, e20453 (2024).
13. Alimagham, S. *et al.* Integrating crop models and machine learning for projecting climate change impacts on crops in data-limited environments. *Agric. Syst.* **228**, 104367 (2025).
14. Mohan, R. N. V. J., Rayanoothala, P. S. & Sree, R. P. Next-gen agriculture: integrating AI and XAI for precision crop yield predictions. *Front. Plant Sci.* **15**, 1451607 (2025).
15. Shahhosseini, M., Hu, G., Huber, I. & Archontoulis, S. V. Coupling machine learning and crop modeling improves crop yield prediction in the US Corn Belt. *Sci. Rep.* **11**, 1606 (2021).
16. Chang, Y., Latham, J., Licht, M. & Wang, L. A data-driven crop model for maize yield prediction. *Commun. Biol.* **6**, 439 (2023).
17. Reichstein, M. *et al.* Deep learning and process understanding for data-driven Earth system science. *Nature* **566**, 195–204 (2019).
18. van Klompenburg, T., Kassahun, A. & Catal, C. Crop yield prediction using machine learning: A systematic literature review. *Comput. Electron. Agric.* **177**, 105709 (2020).
19. Franke, J. A. *et al.* The GGCM Phase 2 emulators: global gridded crop model responses to changes in CO₂, temperature, water, and nitrogen (version 1.0). *Geosci. Model Dev.* **13**, 3995–4018 (2020).
20. van der Hoog, S. Surrogate Modelling in (and of) Agent-Based Models: A Prospectus. *Comput. Econ.* **53**, 1245–1263 (2019).
21. Aderere, M. O., Srivastava, A. K., Butterbach-Bahl, K. & Rahimi, J. Integrating machine learning with agroecosystem modelling: Current state and future challenges. *Eur. J. Agron.* **168**, 127610 (2025).
22. Troost, C., Parussis-Krech, J., Mejail, M. & Berger, T. Boosting the Scalability of Farm-Level Models: Efficient Surrogate Modeling of Compositional Simulation Output. *Comput. Econ.* **62**, 721–759 (2023).

23. Bradford, M. A. *et al.* Managing uncertainty in soil carbon feedbacks to climate change. *Nat. Clim. Change* **6**, 751–758 (2016).
24. Shahhosseini, M., Hu, G., Huber, I. & Archontoulis, S. V. Coupling machine learning and crop modeling improves crop yield prediction in the US Corn Belt. *Sci. Rep.* **11**, 1606 (2021).
25. Zhang, L. *et al.* Planning maize hybrids adaptation to future climate change by integrating crop modelling with machine learning. *Environ. Res. Lett.* **16**, 124043 (2021).
26. Liu, W. *et al.* The statistical emulators of GGCM phase 2: responses of year-to-year variation of crop yield to CO₂, temperature, water, and nitrogen perturbations. *Geosci. Model Dev.* **16**, 7203–7221 (2023).
27. Cereals - European Commission. https://agriculture.ec.europa.eu/farming/crop-productions-and-plant-based-products/cereals_en (2023).
28. Eurostat, Agricultural production - crops. https://ec.europa.eu/eurostat/statistics-explained/index.php?title=Agricultural_production_-_crops (2025).
29. Johnson, S. J. *et al.* SEAS5: the new ECMWF seasonal forecast system. *Geosci. Model Dev.* **12**, 1087–1117 (2019).
30. Hersbach, H. *et al.* The ERA5 global reanalysis. *Q. J. R. Meteorol. Soc.* **146**, 1999–2049 (2020).
31. Cannon, A. J., Sobie, S. R. & Murdock, T. Q. Bias Correction of GCM Precipitation by Quantile Mapping: How Well Do Methods Preserve Changes in Quantiles and Extremes? <https://doi.org/10.1175/JCLI-D-14-00754.1> (2015) doi:10.1175/JCLI-D-14-00754.1.
32. EC. Short-term outlook for EU agricultural markets, Autumn 2022. https://agriculture.ec.europa.eu/system/files/2022-10/short-term-outlook-autumn-2022_en_1.pdf (2022).
33. European Commission. Joint Research Centre. *Drought in Europe: July 2022 : GDO Analytical Report.* (Publications Office, LU, 2022).

34. Barna, F. M. & Manescu, A. C. The Impact of Drought Risk on Maize Crop in Romania. *Sustainability* **17**, 8870 (2025).
35. EC. JRC. *Drought in Europe: July 2022 : GDO Analytical Report*. (Publications Office, LU, 2022).
36. JRC news and updates. https://joint-research-centre.ec.europa.eu/jrc-news-and-updates/summer-drought-keeps-its-grip-europe-2022-08-22_en (2022).
37. Montanari, A. *et al.* Why the 2022 Po River drought is the worst in the past two centuries. *Sci. Adv.* **9**, eadg8304 (2023).
38. van der Velde, M., van Diepen, C. A. & Baruth, B. The European crop monitoring and yield forecasting system: Celebrating 25 years of JRC MARS Bulletins. *Agric. Syst.* **168**, 56–57 (2019).
39. LeCun, Y., Bengio, Y. & Hinton, G. Deep learning. *Nature* **521**, 436–444 (2015).
40. Chung, J., Ahn, S. & Bengio, Y. Hierarchical Multiscale Recurrent Neural Networks. Preprint at <https://doi.org/10.48550/arXiv.1609.01704> (2017).
41. Kingma, D. P. & Ba, J. Adam: A Method for Stochastic Optimization. Preprint at <https://doi.org/10.48550/arXiv.1412.6980> (2017).
42. Huber, P. J. Robust Estimation of a Location Parameter. *Ann. Math. Stat.* **35**, 73–101 (1964).
43. Chollet, F. keras. (2015).
44. Abadi, M. *et al.* TensorFlow: a system for large-scale machine learning. in *Proceedings of the 12th USENIX conference on Operating Systems Design and Implementation* 265–283 (USENIX Association, USA, 2016).
45. Alt, H. & Godau, M. Computing the fréchet distance between two polygonal curves. *Int. J. Comput. Geom. Appl.* **05**, 75–91 (1995).
46. Alt, H. & Scharf, L. Computing the Hausdorff Distance between Curved Objects. *Int J Comput Geom. Appl* **18**, 307–320 (2008).

47. Ridoutt, B. G. *et al.* Area of concern: a new paradigm in life cycle assessment for the development of footprint metrics. *Int. J. Life Cycle Assess.* **21**, 276–280 (2016).
48. Seguini, L., Bussay, A. & Baruth, B. From extreme weather to impacts: The role of the areas of concern maps in the JRC MARS bulletin. *Agric. Syst.* **168**, 213–223 (2019).
49. Voldoire, A. *et al.* Evaluation of CMIP6 DECK Experiments With CNRM-CM6-1. *J. Adv. Model. Earth Syst.* **11**, 2177–2213 (2019).
50. Döscher, R. *et al.* The EC-Earth3 Earth system model for the Coupled Model Intercomparison Project 6. *Geosci. Model Dev.* **15**, 2973–3020 (2022).
51. Dunne, J. P. *et al.* The GFDL Earth System Model Version 4.1 (GFDL-ESM 4.1): Overall Coupled Model Description and Simulation Characteristics. *J. Adv. Model. Earth Syst.* **12**, e2019MS002015 (2020).
52. Ridley, J., Menary, M., Kuhlbrodt, T., Andrews, M. & Andrews, T. MOHC HadGEM3-GC31-MM model output prepared for CMIP6 CMIP. Earth System Grid Federation <https://doi.org/10.22033/ESGF/CMIP6.420> (2019).
53. Müller, W. A. *et al.* A Higher-resolution Version of the Max Planck Institute Earth System Model (MPI-ESM1.2-HR). *J. Adv. Model. Earth Syst.* **10**, 1383–1413 (2018).
54. Seland, Ø. *et al.* Overview of the Norwegian Earth System Model (NorESM2) and key climate response of CMIP6 DECK, historical, and scenario simulations. *Geosci. Model Dev.* **13**, 6165–6200 (2020).

Extended Data

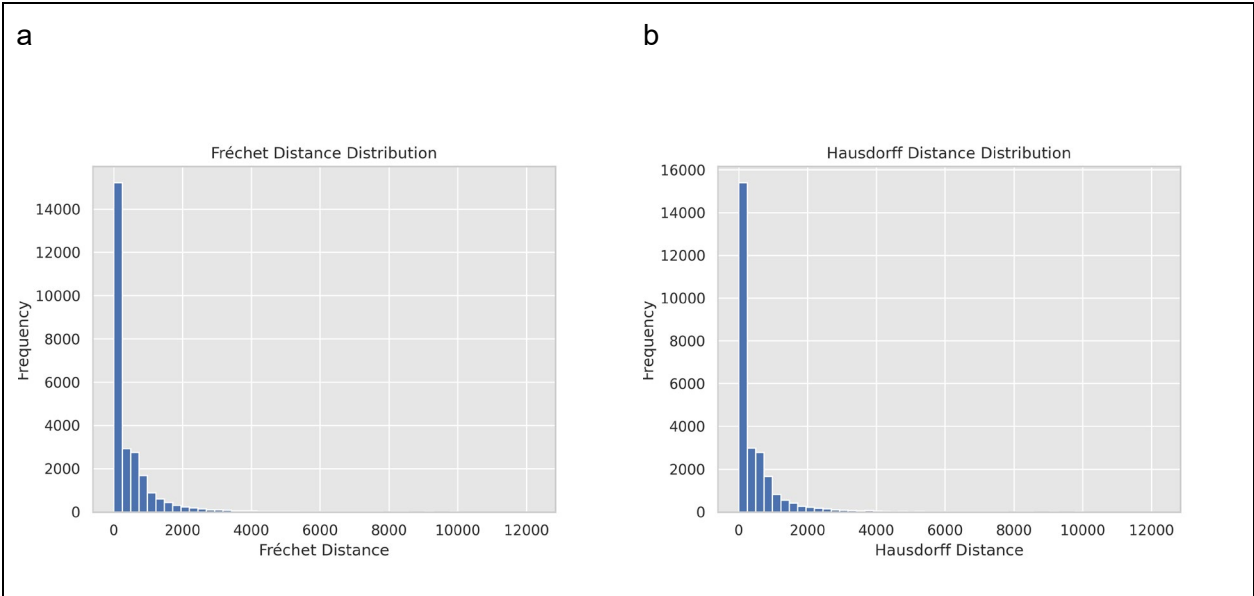
Table A1: CMIP6 historical simulations used with SECS4M, 1993-2014

Model name	Historical realizations	Approximate nominal resolution in degrees (latitude, longitude)	Reference
CNRM-CM6-1-HR	'r1i1p1f2'	0.5°, 0.5°	49
EC-Earth3	'r11i1p1f1', 'r13i1p1f1', 'r15i1p1f1', 'r1i1p1f1', 'r3i1p1f1', 'r4i1p1f1', 'r6i1p1f1', 'r9i1p1f1'	0.7°, 0.7°	50
GFDL-ESM4	'r1i1p1f1'	1°, 1.25°	51
HadGEM3-GC31-MM	'r1i1p1f3'	0.56°, 0.8°	52
MPI-ESM1-2-HR	'r10i1p1f1', 'r1i1p1f1', 'r2i1p1f1', 'r3i1p1f1', 'r4i1p1f1', 'r5i1p1f1', 'r6i1p1f1', 'r7i1p1f1', 'r8i1p1f1', 'r9i1p1f1'	1°, 1°	53
NorESM2-MM	'r1i1p1f1'	1°, 1.25°	54

Table A2: CMIP6 future realizations used to simulate TWSO with SECS4M for AoC generation

Model name	SSP3-7.0	SSP5-8.5
CNRM-CM6-1-HR	-	'r1i1p1f2'

EC-Earth3	'r11i1p1f1', 'r13i1p1f1', 'r15i1p1f1', 'r1i1p1f1', 'r6i1p1f1', 'r9i1p1f1'	'r11i1p1f1', 'r13i1p1f1', 'r15i1p1f1', 'r1i1p1f1', 'r3i1p1f1', 'r4i1p1f1', 'r6i1p1f1', 'r9i1p1f1'
GFDL-ESM4	'r1i1p1f1'	'r1i1p1f1'
HadGEM3-GC31-MM	-	'r1i1p1f3'
MPI-ESM1-2-HR	'r10i1p1f1', 'r1i1p1f1', 'r2i1p1f1', 'r3i1p1f1', 'r4i1p1f1', 'r5i1p1f1', 'r6i1p1f1', 'r7i1p1f1', 'r8i1p1f1', 'r9i1p1f1'	'r1i1p1f1', 'r2i1p1f1'
NorESM2-MM	'r1i1p1f1'	'r1i1p1f1'



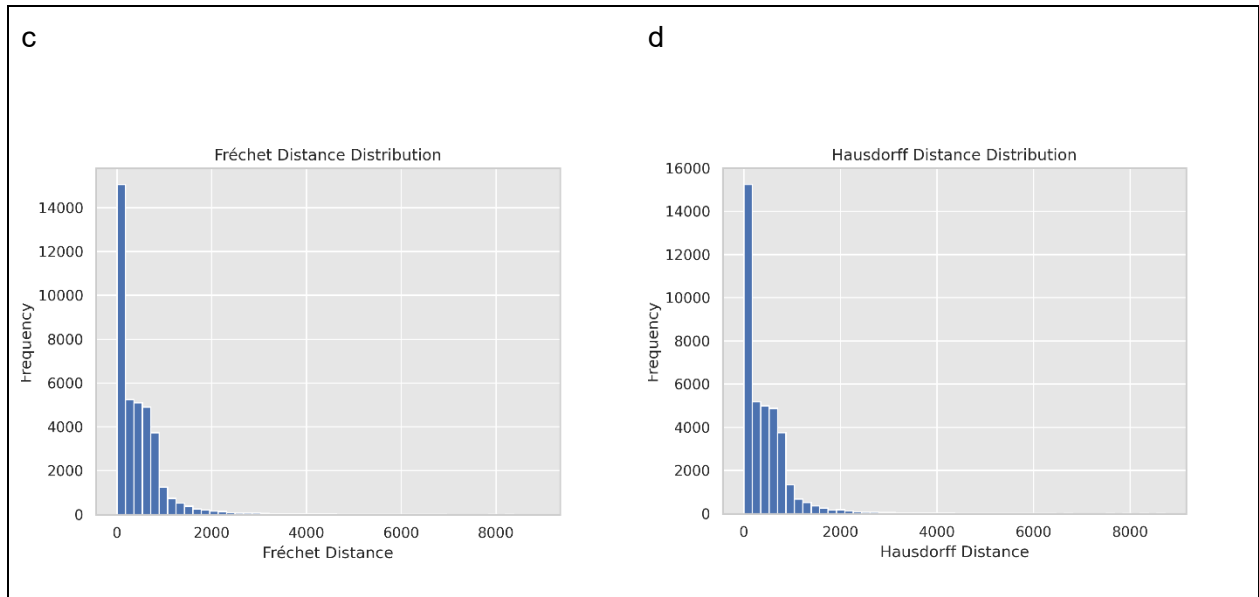


Figure A1: Fréchet and Hausdorff distance distribution histograms for grain maize (a, b) and spring barley (c, d)

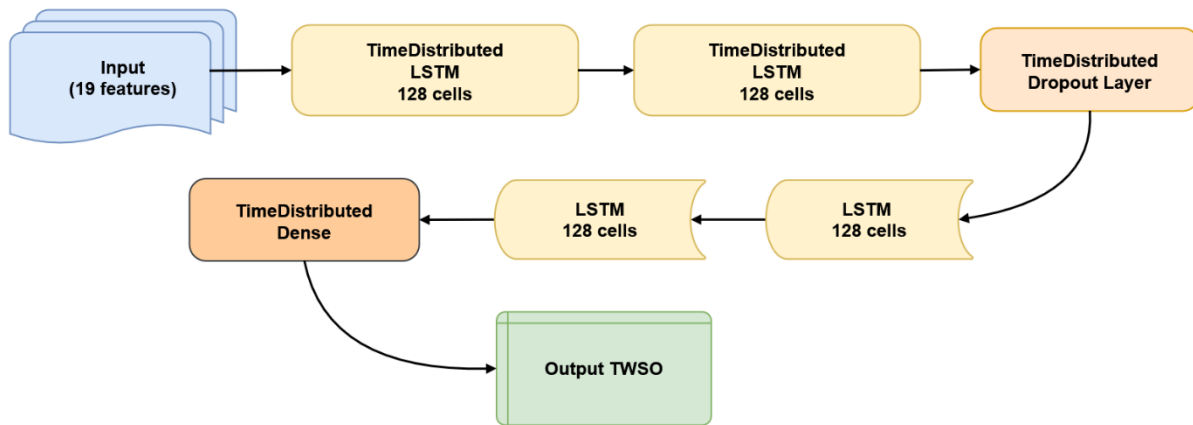


Figure A2: SECS architecture